JBC RESEARCH ARTICLE

Survival and infectivity of second-stage root-knot nematode *Meloidogyne incognita* juveniles depend on lysosome-mediated lipolysis

Received for publication, November 2, 2021, and in revised form, January 3, 2022 Published, Papers in Press, January 24, 2022,
https://doi.org/10.1016/j.jbc.2022.101637

Chao-Jun Lu[1], Yang Meng[1], Yan-Li Wang[2], Tao Zhang[1], Gui-Fang Yang[1], Ming-He Mo[1], Kai-Fang Ji[1], Lian-Ming Liang[1], Cheng-Gang Zou[1,*], and Ke-Qin Zhang[1,*]

From the [1]State Key Laboratory for Conservation and Utilization of Bio-Resources, and [2]Center for Life Sciences, School of Life Sciences, Yunnan University, Kunming, Yunnan, China

Edited by Joseph Jez

Adaptation to nutrient deprivation depends on the activation of metabolic programs to use reserves of energy. When outside a host plant, second-stage juveniles (J2) of the root-knot nematode (*Meloidogyne* spp.), an important group of pests responsible for severe losses in the production of crops (*e.g.*, rice, wheat, and tomato), are unable to acquire food. Although lipid hydrolysis has been observed in J2 nematodes, its role in fitness and the underlying mechanisms remain unknown. Using RNA-seq analysis, here, we demonstrated that in the absence of host plants, the pathway for the biosynthesis of polyunsaturated fatty acids was upregulated, thereby increasing the production of arachidonic acid in middle-stage J2 *Meloidogyne incognita* worms. We also found that arachidonic acid upregulated the expression of the transcription factor *hlh-30b*, which in turn induced lysosomal biogenesis. Lysosomes promoted lipid hydrolysis *via* a lysosomal lipase, LIPL-1. Furthermore, our data demonstrated that blockage of lysosomal lipolysis reduced both lifespan and locomotion of J2 worms. Strikingly, disturbance of lysosomal lipolysis resulted in a decline in infectivity of these juveniles on tomato roots. Our findings not only reveal the molecular mechanism of lipolysis in J2 worms but also suggest potential novel strategies for the management of root-knot nematode pests.

Plant parasitic nematodes infest over 2000 cultivated crops and cause annual economic loss of approximate US $157 billion (1). Among the plant parasitic nematodes, *Meloidogyne* spp. cause root knots in a wide range of hosts across broad geographic areas. There are four common pest species of root-knot nematodes (RKNs): *Meloidogyne incognita*, *Meloidogyne arenaria*, *Meloidogyne javanica*, and *Meloidogyne hapla*. These four species are responsible for the majority of nematode-induced crop losses (2). With an increasing ban of chemical nematicides during the last 2 decades, developing novel control agents has become an urgent need to mitigate the damages by RKNs (3, 4).

Like the free-living nematode *Caenorhabditis elegans*, the life cycle of RKNs consists of the egg, four juveniles, and adult stages (5). The hatching of second-stage juveniles (J2) of RKNs mainly depends on moisture and temperature, without the need of host root diffusates (6). As obligate endo-parasites, the infective J2 of RKNs must infect a host plant to obtain food and ensure subsequent reproduction. However, before infecting host plants, J2 worms have no external food intake. Thus, understanding the underlying mechanisms of J2 worms survival before infection (*i.e.*, when they are outside of the host plants) is essential for developing appropriate control measures against these nematodes (6).

Lipid reserves in nematodes are mainly composed of neutral lipids (especially triglycerides) (7). In *C. elegans*, L4 larva and young adult worms can maintain whole-body energy homeostasis by promoting lipid hydrolysis in response to nutrient deprivation (8–10). For instance, the transcription factor HLH-30 (the ortholog of mammalian transcription factor EB [TFEB]) is a master regulator of autophagy and lysosomal biogenesis in response to nutritional cues. The expression of *hlh-30* is induced in *C. elegans* during nutrient deprivation (9). HLH-30 then upregulates lysosomal lipases, such as LIPL-1 and LIPL-3, thereby eliciting lysosomal lipolysis. Our previous study has demonstrated that octopamine elicits lipid hydrolysis by inducing the expression of the lipase gene *lips-6*, allowing worms to survive during starvation (10). In J2 worms of RKNs, consumption of lipid storage has been observed (11, 12). The survival duration of J2 worms seems to be positively correlated with lipid content (6, 13, 14). Furthermore, a decrease in lipid reserve yields an obvious reduction in locomotor activity of infective juveniles (14, 15). In addition, the infectivity of *Meloidogyne* spp. declines significantly with a corresponding decrease of lipid reserve (11, 16).

At present, the molecular mechanism of lipid breakdown in J2 worms when they are outside of the host plants remains unclear and represents a gap of knowledge in the field. Using RNA-seq analysis, we reported here that lysosomal activity was induced by the transcription factor HLH-30B in J2 of *M. incognita* in the absence of host plants. Lysosome in turn promoted lipid hydrolysis *via* a lysosomal lipase, LIPL-1. The

* For correspondence: Cheng-Gang Zou, chgzou@ynu.edu.cn; Ke-Qin Zhang, kqzhang@ynu.edu.cn.

expression of *hlh-30b* was upregulated by an ω-6 polyunsaturated fatty acid (PUFA), arachidonic acid (AA). Finally, our results demonstrated that lysosomal lipolysis was beneficial for J2 survival and mobility in the absence of host plants. Either blockage or depletion of lysosomal lipolysis could reduce the infectivity of J2 worms on tomato roots.

Results

Transcriptome analysis of J2 worms in the absence of host plants

In the absence of host plants, *M. incognita* J2 started to die around day 6 and the maximum lifespan was around 25 days at 28 °C (Fig. 1*A*). Using Nile Red staining, we found that the quantity of fat granules was reduced by approximately 73% and 93% in 9-day-old (middle-stage) and 19-day-old J2 worms (late-stage), respectively, compared with those in 2-day-old J2 worms (early-stage) (Fig. 1, *B* and *C*). Similar results were obtained by Oil Red O (Fig. S1, *A* and *B*) and Sudan Black staining (Fig. S1, *A* and *C*). Thus, lipid hydrolysis increased in J2 of *M. incognita* with age, consistent with the observation that J2 worms consume stored fat granules in the absence of host plants (6, 13). To clarify the mechanism of lipolysis in J2 worms, we used RNA-seq analysis to compare the transcriptional profiles of middle-stage *versus* early-stage J2 worms (Table S1). These genes represented a broad transcriptional response in J2 worms outside host plants. A gene set enrichment analysis (GSEA) revealed enrichment of the gene set associated with the KEGG term "lysosome" and "biosynthesis of unsaturated fatty acids" in J2 worms at the middle-age stage *versus* the early-age stage (Fig. 1, *D* and *E*). Thus, these pathways are likely involved in physiological responses in J2 worms when they are outside host plants.

HLH-30B promotes lysosomal activity in J2 worms

As the KEGG pathway "lysosome" was overrepresented among the upregulated genes, we tested lysosomal activity in J2 worms using two dyes, LysoTracker Red and LysoTracker Green. Both fluorescence intensity and the amount of puncta were used to represent lysosome activity (17–19). We found that both fluorescence intensity and the number of LysoTracker Red-positive puncta were significantly increased in middle-stage J2 worms, compared with those in early-stage J2 worms (Fig. 2, *A*–*C*). Similar results were obtained from staining with LysoTracker Green (Fig. S2, *A*–*C*). Using quantitative real-time PCR (qPCR), we determined the mRNA levels of several genes encoding lysosomal proteases, such as *cpr-3*, *cpr-4*, *cpz-1*, and a lysosomal hydrolase *lipl-1*. We found that their transcript levels were markedly upregulated in middle-stage J2 worms (Fig. 2*D*). These results suggest that lysosomal activity is increased in J2 worms with increasing age.

TFEB/HLH-30 is a master regulator of lysosome- and autophagy-related genes in mammals and worms (20–22).

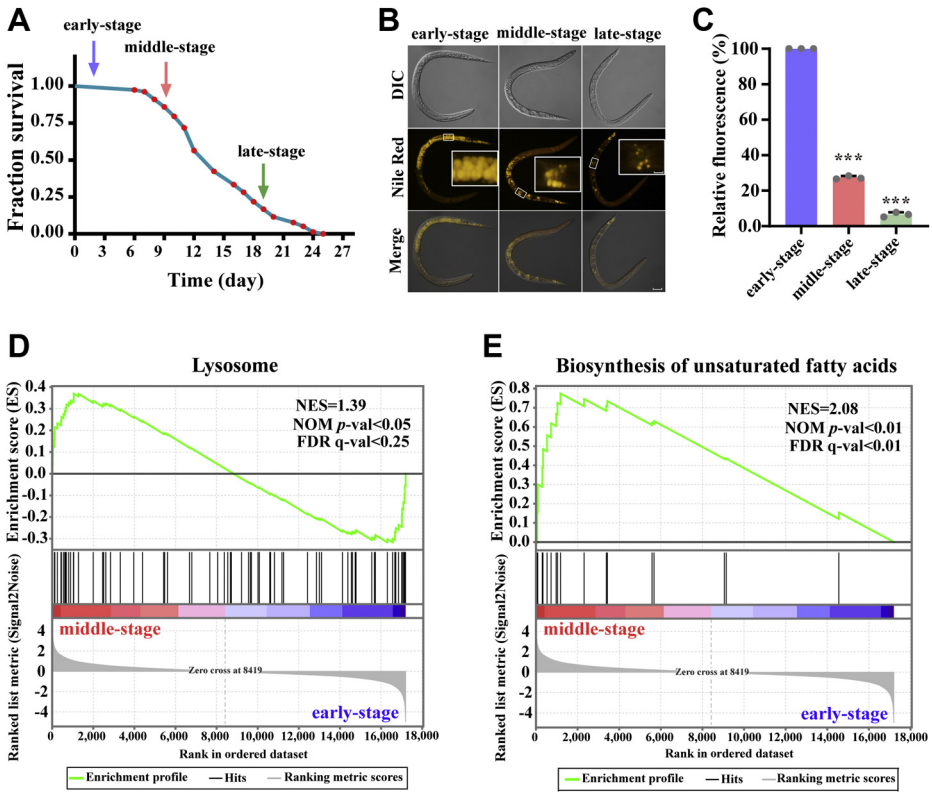

Figure 1. Lipid is mobilized in J2 worms in the absence of hosts. *A*, survival rate of *Meloidogyne incognita* J2 worms in the absence of a host plant. Early-stage: 2-day-old, middle-stage: 9-day-old, and late-stage: 19-day-old. *B*, to assess lipid contents, postfixed J2 worms were stained with Nile Red. The scale bar represents 16 μm. The insertion bar represents 5 μm. *C*, quantification of relative fluorescence of Nile Red. ***$p < 0.001$. *D* and *E*, a GSEA plot showing enrichment of the gene set associated with the KEGG term "lysosome" (*D*) and "biosynthesis of unsaturated fatty acids" (*E*) in J2 worms at the middle-stage *versus* the early-stage. GSEA, gene set enrichment analysis; J2, second-stage juveniles.

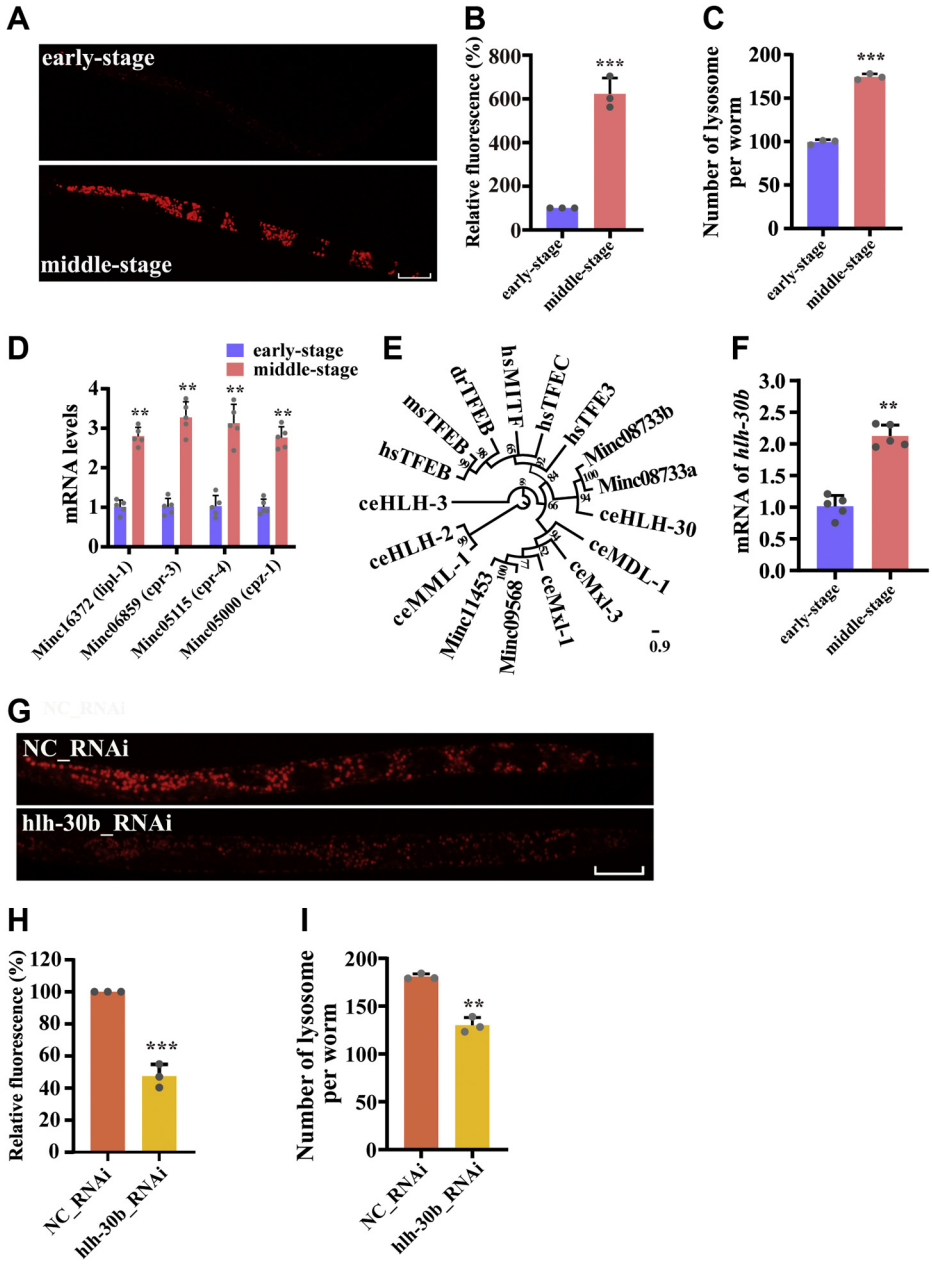

Figure 2. HLH-30B promotes lysosomal activity in J2 worms. *A*, lysosome was stained with LysoTracker Red (LR) in early-stage and middle-stage J2 worms. The scale bar represents 20 μm. *B*, quantification of relative fluorescence of LR. *C*, quantification of LR puncta. *D*, expression of lysosomal genes in early-stage and middle-stage J2 worms. *E*, phylogenetic relationship of TFEB/HLH-30. *F*, the expression of *hlh-30b* was upregulated in middle-stage J2 worms, compared to that in early-stage J2 worms. *G*, knockdown of *hlh-30b* by RNAi-suppressed lysosomal activity stained with LR in middle-stage J2 worms. The scale bar represents 20 μm. *H*, quantification of relative fluorescence of LR. *I*, quantification of LR puncta. $^{**}p < 0.01$; $^{***}p < 0.001$. ce, *Caenorhabditis elegans*; dr, *Danio rerio*; hs, *Homo sapiens*; J2, second-stage juveniles; mm, *Mus musculus*; NC, negative control.

Meloidogyne incognita possesses two homologs of *C. elegans* HLH-30 and mammalian TFEB, namely Minc08733a and Minc08733b, which contain highly conserved helix-loop-helix DNA-binding domain (Fig. S3). Phylogenetic analysis further revealed that both Minc08733b and Minc08733a were clustered into the sub-group of HLH-30 and TFEB (Fig. 2*E*). However, RNA-seq analysis revealed that only Minc08733b (*hlh-30b*) expression was detected and induced in middle age J2 worms (Table S1). These results were confirmed by qPCR (Fig. 2*F*). To investigate whether *hlh-30b* regulated lysosomal activity in J2 worms, we knocked down this gene by RNAi (Fig. S4*A*). Worms treated with *hlh-30b* RNAi displayed decreases in fluorescence intensity and in the amount of LysoTracker Red-positive puncta (Fig. 2, *G–I*). These findings suggest that lysosome activity is induced *via* HLH-30B in J2 worms in the absence of host plants.

Lipolysis in J2 worms is mediated by lysosome via *a lysosomal lipase, LIPL-1*

Using transmission electron microscopy, we observed the intestinal structure of J2 worms. Consistent with a previous

study (23), the lipid droplets of greyish compartments marked with red shuriken were almost filled in the corresponding cross section of intestine in early-stage J2 worms (Fig. 3, *A* and *B*). In contrast, charcoal gray lysosome granules labeled with green dotted cycles were scarce in early-stage J2 worms. However, the number of lysosome granules was significantly increased accompanied with a decrease in lipid droplets in middle-stage J2 worms, compared with those in early-stage J2 worms (Fig. 3, *A* and *B*). These results implicate that lysosome function is associated with lipid hydrolysis in J2 worms when they were outside of host plants. To test this hypothesis, the lysosome activity was blocked by two lysosome inhibitors, chloroquine (320 μM) and NH_4Cl (10 μM). We found that these two inhibitors substantially suppressed lipid hydrolysis in J2 worms (Fig. 3, *C* and *D*). Furthermore, knockdown of *hlh-30b* by RNAi also reduced lipolysis (Fig. 3, *E* and *F*). Together, these results indicate that lipid hydrolysis is mediated by lysosome, but the mechanism underlying uptake of lipids into the lysosomes remains unclear. A recent study demonstrated that the interactions between the lysosomes and lipid droplets led to the transfer of lipids from lipid droplets directly into the lysosomes in hepatocytes (24). In this study, we also observed that lipid droplets labeled with Nile Red interacted with the lysosomes stained by LysoTracker Green (Fig. 3*G*).

As mentioned above, qPCR analysis revealed an increase in the mRNA levels of *lipl-1* encoding lysosomal acid lipase in middle-stage J2 worms, compared with those in early-stage J2 worms (Fig. 2*D*). In *C. elegans*, HLH-30 upregulates the expression of *lipl-1* during starvation (9, 25). HLH-30 has been shown to bind the E-box motif (CACGTG) *in vitro* (25). In the *lipl-1* promoter, there is a CACGAG hexamer element (upstream of ATG), which is a putative HLH-30 binding site (Fig. S5). Indeed, knockdown of *hlh-30b* by RNAi markedly reduced the *lipl-1* expression in middle-stage J2 worms (Fig. 3*H*). To investigate the role of *lipl-1* in lysosomal lipolysis, we silenced this gene by RNAi (Fig. S4*B*). Knockdown of *lipl-1* markedly suppressed lipid hydrolysis (Fig. 3, *I* and *J*), rather than lysosome activity (Fig. S6, *A*–*C*). These results suggest

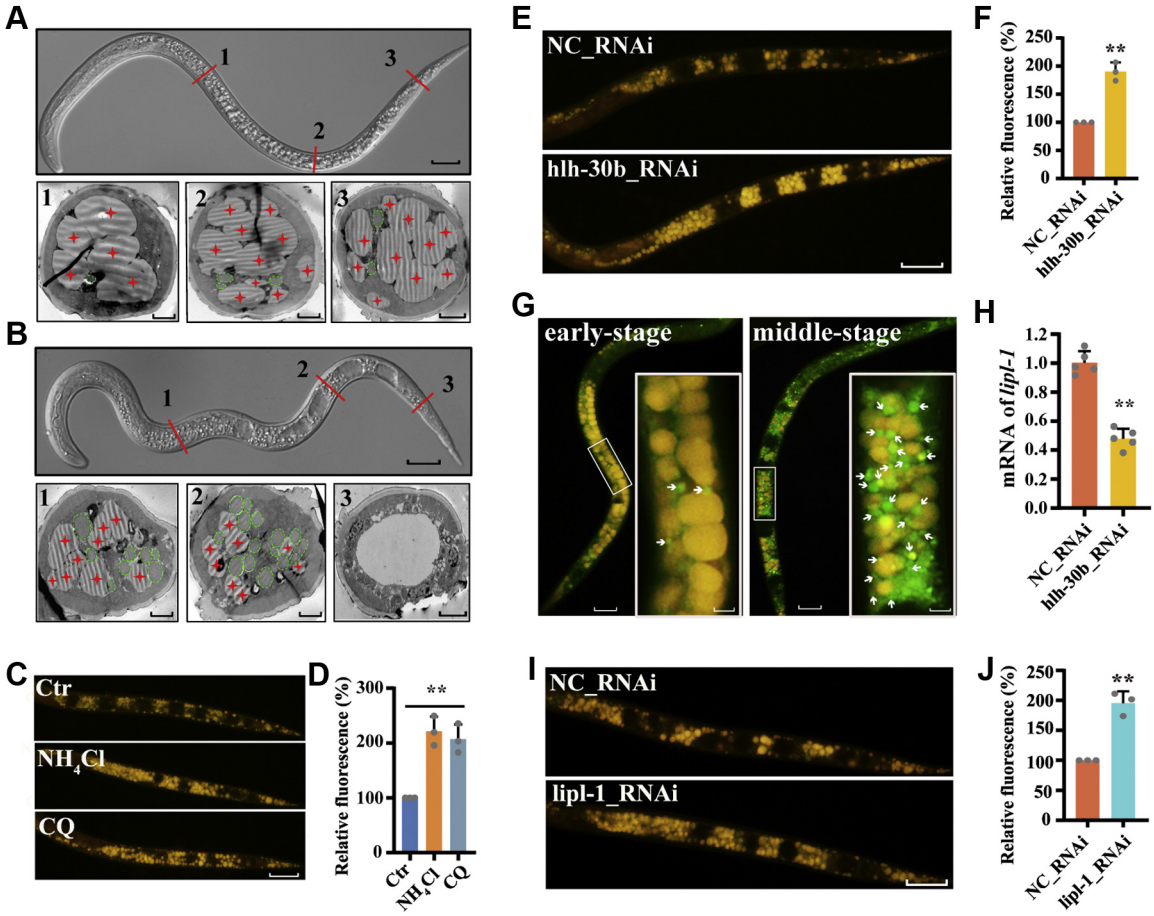

Figure 3. Lipolysis in J2 worms is mediated by lysosome *via* a lysosomal lipase, LIPL-1. *A* and *B*, electron micrographs of cross-sections of the anterior and the posterior portions of early- (*A*) and middle-stage (*B*) of J2 worms in the absence of a plant host. Electron micrographs of 1, 2, and 3 refer to the cross sections of anterior, middle, and posterior of the intestine in J2 worms. *Grayish* and ruga areas marked with *red shuriken* indicated lipid droplets. *Charcoal gray areas* labeled with *green dotted cycle* referred to lysosomes. The scale bar represents 20 μm. The inserction bar represents 3.6 μm. *C*, treatment with lysosome inhibitors, NH_4Cl (10 μM), and chloroquine (CQ, 320 μM), led to a significant decrease in the lipolysis of J2 worms. Lipid droplets were stained with Nile Red. The scale bar represents 20 μm. *D*, quantification of the relative fluorescence of Nile Red. *E*, knockdown of *hlh-30b* resulted in a significant decline in lipolysis. Lipid droplets were stained with Nile Red. The scale bar represents 20 μm. *F*, quantification of the relative fluorescence of Nile Red. *G*, lipid droplets were stained with Nile Red (*yellow*) and the lysosomes were stained with LysoTracker Green (*green*). The scale bar represents 16 μm. The insertion bar represents 4.5 μm. *H*, knockdown of *hlh-30b* suppressed the expression of *lipl-1*. *I*, knockdown of *lipl-1* significantly inhibited lipolysis in J2 worms. The scale bar represents 20 μm. *J*, quantification of the relative fluorescence of Nile Red. $^{**}p < 0.01$. Ctr, the control group; NC, negative control; J2, second-stage juveniles.

that the breakdown of lipid droplets is mediated by lysosomal lipolysis *via* LIPL-1 in J2 worms in the absence of host plants.

Arachidonic acid promotes lysosomal activity via *HLH-30B*

In this study, the KEGG pathway "biosynthesis of unsaturated fatty acids" was also significantly enriched, implicating that the biosynthesis of PUFAs is probably increased in middle-stage J2 worms. The "stearoyl-CoA 9-desaturase activity" genes, such as Minc00222 (an ortholog of *C. elegans* △9 desaturase *fat-6*), Minc10964 (the orthologs of *C. elegans* △5 desaturase *fat-4*), Min00824 (an ortholog of *C. elegans* △6 desaturase *fat-3*), and Min12955 (an ortholog of *C. elegans* elongase *elo-1*) (Fig. S7, *A* and *B*), were all significantly upregulated in middle-stage J2 worms, which were confirmed by qPCR (Fig. 4*A*). In *C. elegans*, FAT-6, FAT-3, and FAT-4 desaturases catalyze the conversion of C18:0, C18:2n6, and C20:3n6 into C18:1n9, C18:3n6, and C20:4n6 PUFAs, respectively, whereas ELO-1 elongates C18 to C20 PUFAs (26). As the expressions of these PUFA biosynthesis-related genes were increased, we determined fatty acid composition profile in J2 worms by GC-MS. Gas chromatography/mass spectrometry analysis revealed that compared to those in early-stage J2 worms, the contents of two ω-6-PUFAs dihomo-γ-linolenic acid (C20:3n6) and AA (C20:4n6) and two ω-3-PUFAs eicosatetraenoic acid (C20:4n3) and eicosapentaenoic acid (C20:5n3) were remarkably increased in middle-stage J2 worms (Fig. 4*B*).

Next, we tested whether these PUFAs were involved in enhanced lysosomal activity. We found that supplementation with 100 μM of AA, but not dihomo-γ-linolenic acid, eicosatetraenoic acid, and eicosapentaenoic acid, increased the fluorescence intensity of LysoTracker Red in J2 worms (Fig. S8). Furthermore, the fluorescence intensity of LysoTracker Red was significantly reduced in middle-stage J2 worms subjected to *fat-6* and *fat-3* RNAi (Figs. 4, *C* and *D* and S4*C*). However, supplementation with AA rescued the decrease in the fluorescence intensity of LysoTracker Red in middle-stage J2 worms after knockdown of *fat-6* and *fat-3* by RNAi (Fig. 4, *C* and *D*). Moreover, knockdown of either *fat-6* or *fat-3* led to a decrease in the mRNA levels of *hlh-30b* in middle-stage J2 worms (Fig. 4*E*). Such suppression could be restored by supplementation with AA. Finally, we found that RNAi knockdown of *hlh-30b* inhibited the fluorescence intensity of LysoTracker Red in middle-stage J2 worms (Fig. 4, *F* and *G*). However, supplementation with AA failed to restore the reduction of fluorescence intensity of LysoTracker Red in middle-stage J2 worms subjected to *hlh-30b* RNAi. It should be noted that supplementation with a saturated fatty acid, palmitic acid (100 μM), did not affect the fluorescence intensity of LysoTracker Red in J2 worms (Fig. S8). These results indicate that AA promotes lysosome activity *via* upregulating *hlh-30b*.

Role of lipid hydrolysis in the survival and mobility of J2 worms

To investigate the role of lipid hydrolysis in the survival of J2 worms, lipid hydrolysis was inhibited by treatment with NH_4Cl or by either *hlh-30b* or *lipl-1* RNAi in J2 worms. A significant decrease in median lifespan was observed in J2 worms after NH_4Cl treatment or knockdown of either *hlh-30b* or *lipl-1* (Fig. 5, *A*–*C*). Next, we monitored the mobility of J2 worms after inhibition of lipolysis. Treatment with NH_4Cl or knockdown of either *hlh-30b* or *lipl-1* by RNAi led to a significant decrease in body bending and migration ability in middle-stage J2 worms (Fig. 5, *D*–*I*). These results suggest that lipid hydrolysis is required for maintaining fitness in J2 worms in the absence of host plants.

Intervention of lipolysis suppresses infectivity of J2 worms

As body bending and migration of J2 worms are important determinants for their infectivity (27), we hypothesized that blockage of lipid hydrolysis could suppress the infection of J2 worms with a host plant. To test this hypothesis, J2 worms were pretreated with NH_4Cl for 6 days and allowed to infect tomato roots. Indeed, treatment of J2 worms with NH_4Cl significantly blocked lipid hydrolysis and resulted in ∼60% decrease in infectivity on tomato roots (Figs. S9*A* and 6, *A* and *B*). Similarly, blockage of lipid hydrolysis induced by *lipl-1* RNAi also yielded a decline in infectivity by approximately 36% (Figs. S9*B* and 6, *C* and *D*).

Previous studies have shown that lipid contents are correlated with the infectivity of J2 worms (11, 16, 28). As expected, the infectivity of J2 worms on tomato roots was reduced to about 39% and 11% in middle- and last-stage J2 worms, respectively, compared to that of early-stage J2 worms (Fig. 6, *E* and *F*). As mentioned above, the lipid contents were approximately 27% and 7% in middle- and last-stage J2 worms, compared to those in early-stage J2 worms (Fig. 1, *B* and *C*). Thus, there seemed a positive correlation between the lipid content and the infectivity of J2 worms on tomato roots. This correlation led us to hypothesize that accelerated lipolysis by chemical intervention could reduce the infectivity of J2 worms. To test this hypothesis, early-stage J2 worms were treated with AA (100 μM). After treatment with AA for 6 days, J2 worms had approximately 71.5% lipid contents (*versus* J2 worms treated with vehicle) (Fig. S9*C*). Compared to J2 worms treated with vehicle (ethanol), only about 65.5% of the J2 worms treated with AA was able to infect the roots of tomato. In contrast, supplementation with palmitic acid did not influence the lipid contents and infectivity (Figs. S9*C* and 6, *G* and *H*). Taken together, these results suggest that disturbance of lysosomal lipolysis can be a novel alternative for the management of RKNs.

Discussion

Lipid hydrolysis has been commonly observed in J2 of RKNs in the absence of host plants (11, 16, 28). Here, we elucidated the molecular mechanism of lipid hydrolysis, which is required for maintaining fitness of J2 worms when they are outside of host plants (Fig. 7). Disturbance of lipolysis reduces the infectivity of J2 worms on tomato roots, suggesting that intervention of lipolysis is a promising approach for protecting host plants against nematode infections. Thus, understanding

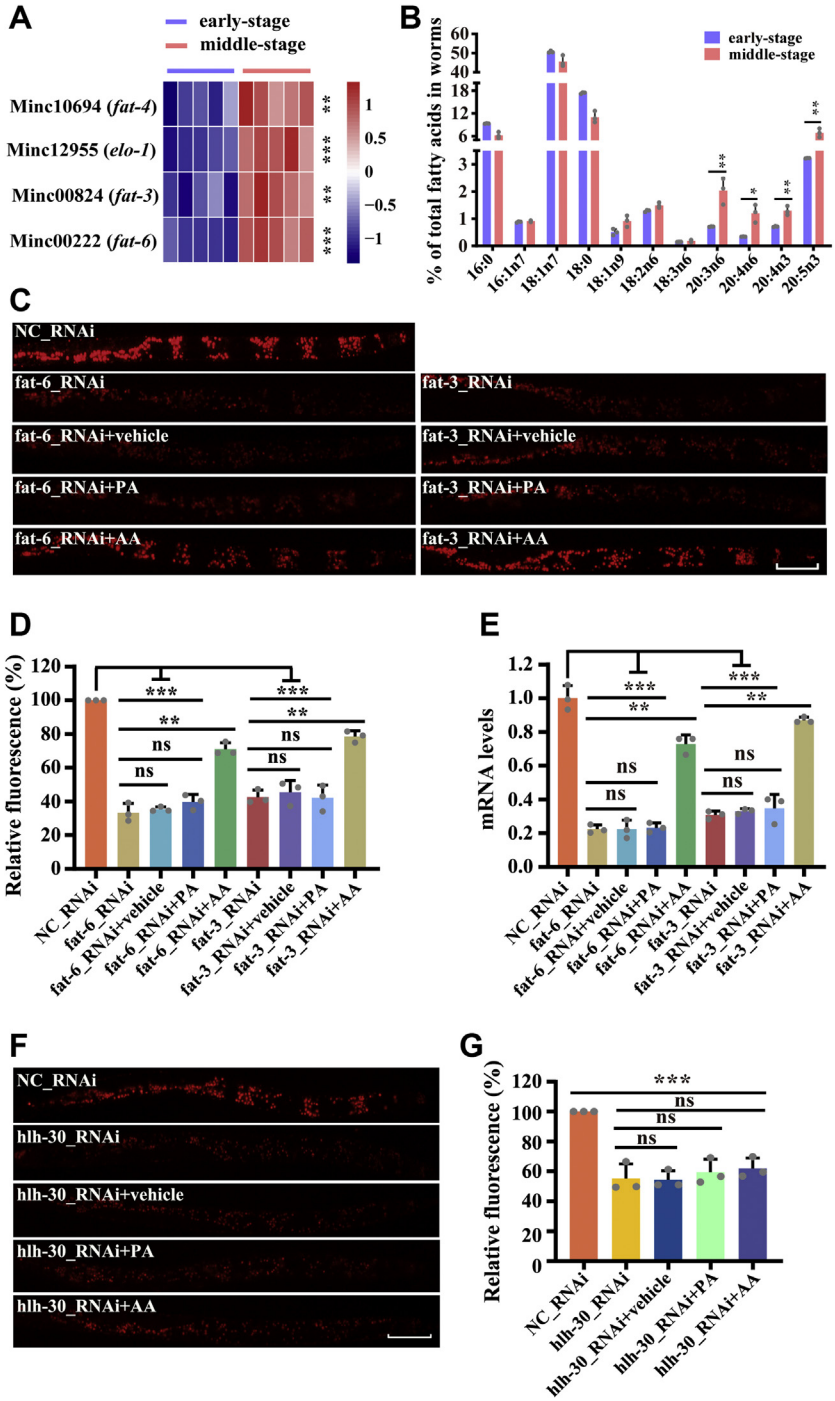

Figure 4. Arachidonic acid is involved in the biogenesis of lysosome. *A*, hierarchical clustering of the expression levels of fatty acid desaturase and fatty acid elongase genes detected by qPCR. *B*, the contents of four polyunsaturated fatty acids in middle-stage J2 worms were higher than those in early-stage J2 worms. *C*, the activity of lysosome was inhibited in J2 worms subjected to *fat-6* or *fat-3* RNAi, which was rescued by supplementation with arachidonic acid (AA), but not palmitic acid (PA). Lysosome was stained with LysoTracker Red (LR) in J2 worms. The scale bar represents 20 μm. *D*, quantification of the relative fluorescence of LR. *E*, the expression of *hlh-30b* was controlled by AA but not PA. *F*, supplementation with either AA or PA failed to rescue a decrease in lysosomal activity in J2 worms subjected to *hlh-30b* RNAi. The scale bar represents 20 μm. *G*, quantification of relative fluorescence of LR. $^{**}p < 0.01$; $^{***}p < 0.001$; NC, negative control; ns, not significant; J2, second-stage juveniles.

the molecular mechanisms involved in lipolysis in J2 worms will contribute to developing strategies to reduce damages by RKNs.

In this study, our data revealed that an increase in lysosomal activity was accompanied by a decrease in lipid contents with age implicating a positive correlation between lysosomal function and lipid hydrolysis. Our results indicate that the expression of *hlh-30b* is upregulated, leading to an increase in lysosome activity in middle-stage J2 worms. Concomitantly, the activation of lysosome promotes lipid hydrolysis *via* a lysosomal lipase, LIPL-1, in middle-stage J2 worms. A similar mechanism has been proposed in adult *C. elegans*

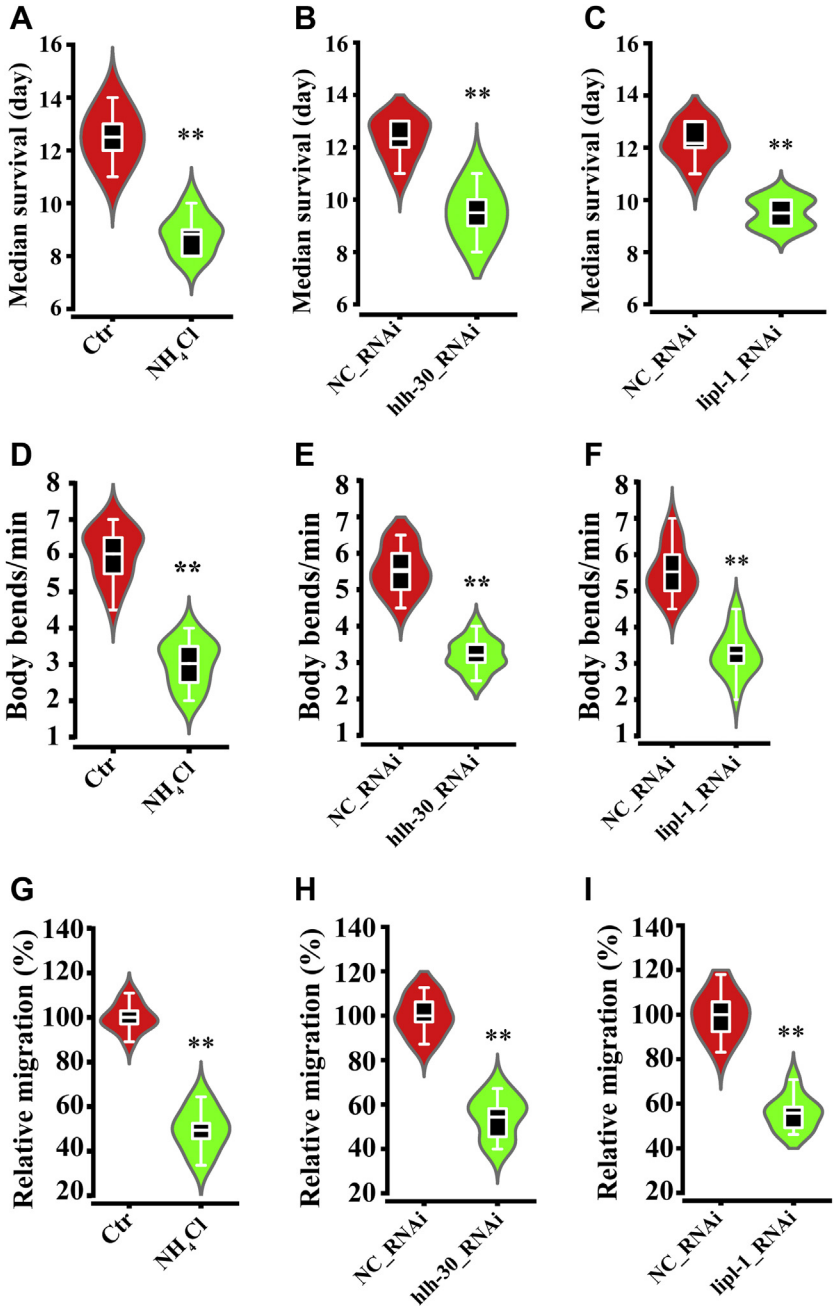

Figure 5. Blockage of lipid hydrolysis shortens lifespan and reduces the mobility of J2 worms. *A–C*, supplementation with NH_4Cl (*A*) or RNAi knockdown of either *hlh-30b* (*B*) or *lipl-1* (*C*) reduced the median lifespan in J2 worms. *D–F*, supplementation with NH_4Cl (*D*) or RNAi knockdown of either *hlh-30b* (*E*) or *lipl-1* (*F*) reduced body bending in J2 worms. *G–I*, supplementation with NH_4Cl (*G*) or RNAi knockdown of either *hlh-30b* (*H*) or *lipl-1* (*I*) reduced the migration of J2 worms. $^{**}p < 0.01$. Ctr, the control group; J2, second-stage juveniles; NC, negative control.

hermaphrodites (9). Starvation activates HLH-30 by upregulating its expression and inducing its nuclear translocation. The activated HLH-30 in turn promotes lysosomal lipolysis through the induction of lysosomal lipases in *C. elegans*. These results suggest a conserved role for HLH-30 in lysosomal lipolysis in worms.

It has been reported that mutations in *hlh-30* lead to more than 50% reduction in lifespan in *C. elegans* under starvation conditions (9, 29). Our results demonstrate that blockage of lysosomal lipolysis by either knockdown of *hlh-30b* or treatment with lysosome inhibitor NH_4Cl remarkably reduces the median lifespan, mobility, and migration in J2 worms. Thus, lysosomal lipolysis is required for the survival of J2 worms in the absence of host plants.

Our results demonstrate that the upregulation of PUFA biosynthesis-related genes, such as *fat-3* and *fat-6*, results in an increase in the production of PUFAs, such as AA, in middle-stage J2 worms. Knockdown of *fat-3* or *fat-6* inhibits the upregulation of *hlh-30b*, which is restored by AA supplementation. Thus, AA serves as an upstream molecule to regulate *hlh-30b*. How AA induces the transcription of *hlh-30b* is not clear yet. In mammalian cells, TFEB activity is regulated

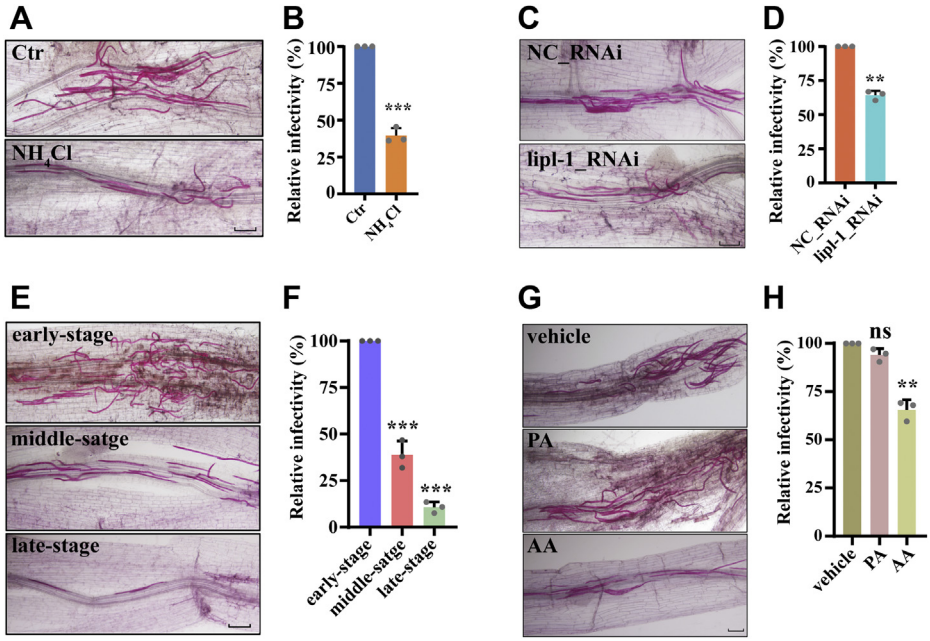

Figure 6. Intervention of lipolysis restrains the infectivity of J2 worms on tomato roots. *A* and *B*, treatment with NH_4Cl reduced the infectivity of J2 worms. The scale bar represents 200 μm. *C* and *D*, knockdown of *lipl-1* by RNAi inhibited the infectivity of J2 worms. The scale bar represents 200 μm. *E* and *F*, the infectivity of J2 worms was reduced in middle- and late-stage J2 worms, compared to that of early-stage J2 worms. The scale bar represents 200 μm. *G* and *H*, J2 worms pretreated with arachidonic acid (AA), but not palmitic acid (PA), for 6 days exhibited a significant drop in infectivity. The scale bar represents 175 μm. *A*, *C*, *E*, and *G*, photographs displayed J2 worms within tomato roots after 36 h infection. *B*, *D*, *F*, and *H*, quantification of relative infectivity. $^{**}p < 0.01$; $^{***}p < 0.001$. Ctr, the control group; J2, second-stage juveniles; NC, negative control.

at both the transcriptional and posttranscriptional levels by nutrient availability (29). For example, starvation promotes TFEB nuclear translocation. TFEB in the nucleus then modulates its own expression by a positive transcriptional autoregulatory mechanism (29). Likewise, HLH-30 also regulates its own transcription in *C. elegans* during fasting (9). Beside transcriptional autoregulation of TFEB/HLH-30, the nuclear hormone receptor (NHR) peroxisome proliferator activated

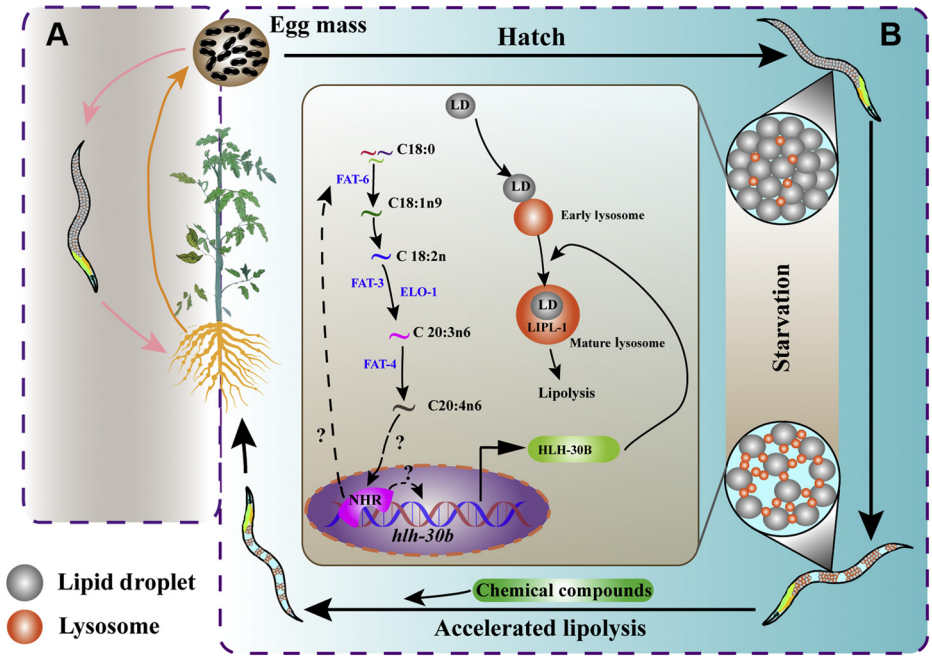

Figure 7. Schematic representation of a potential strategy for controlling RKNs by promoting lipolysis. In the presence of plant hosts (*A*), newly hatched J2 worms usually infect the roots of plants. In the absence of plant hosts (*B*), J2 worms hatched from eggs reside in fields and suffer from starvation. During starvation, the increased abundance of polyunsaturated fatty acids upregulated the expression of *hlh-30b* probably through an unknown nuclear hormone receptor (NHR), leading to an increase in lysosomal activity. The activation of lysosome in turn triggers lipolysis *via* the lysosomal lipase LIPL-1. If lipolysis is accelerated by chemical intervention, the infectivity of J2 worms on plant roots is reduced. Thus, promoting lipolysis is likely to be a novel target of RKN control. RKNs, root-knot nematodes.

receptor (PPARα) is also involved in the regulation of TFEB expression in the liver during starvation (30). A recent study revealed that a long chain fatty acid oleoylethanolamide bound to the NHR-80, thereby initiating lysosome biogenesis in *C. elegans* (31). Although NHRs, such as NHR-80 and NHR-49, are homologous to the mammalian NHR, HNF-4 (32), it is believed that their functions are similar to those of peroxisome proliferator activated receptor (33, 34). It is well-established that long chain fatty acids are endogenous ligands for HNF-4 (35, 36). It is thus tempting to speculate that AA might act as a ligand of a NHR to mediate the transcription of *hlh-30b* in J2 worms. However, the number of NHRs in the *M. incognita* genome is 92 (5), making it difficult to identify which specific NHR may bind to PUFAs.

Our study indicates that either blockage of lysosomal lipolysis by NH_4Cl or the activation of lysosomal lipolysis by AA can suppress the infectivity of J2 worms on tomato roots. These observations suggest the potential adoption of control measures against RKNs based on inhibiting or accelerating fat mobilization. Indeed, ammonia-releasing compounds, such as $(NH_4)_2CO_3$ and $(NH_4)_2SO_4$, have been used against a variety of the plant-parasitic nematodes (37–39). Although treatment of NH_4Cl reduces the lifespan of J2 worms, it has a relatively weak nematicidal activity. Based on our observation, the action of ammonia-releasing compounds to control RKNs is mainly attributed to reduce the infectivity of J2 worms by inhibiting lysosomal lipolysis. For J2 worms, synchronization between hatching from eggs and the presence of suitable roots nearby is desirable in the establishment of a successful parasitic relationship (16). However, hatching of infective J2 worms is often not synchronized with the occurrence of susceptible host roots (40). Our results demonstrate that AA reduces the infectivity of J2 worms by accelerating lysosomal lipolysis, suggesting that compounds that are capable of inducing lysosomal lipolysis can also be applied to reduce the infectivity of J2 worms. Based on these results, we propose the following approach toward RKN control as outlined in Figure 7. Before crops are planted in a field, an inducer is added into the field to promote rapid lipolysis in J2 worms. After the lipid contents of J2 worms are greatly decreased around a week, the crops can be seeded. However, the effectiveness of this approach in crop field conditions awaits further experimental testing.

Experimental procedures

Maintenance and collection of nematodes

J2 worms of *M. incoganita* were maintained and collected according to the method described previously (5). For RNA-seq analysis, the early-stage and middle-stage J2 worms were kept in 0.25× M9 buffer for 2 and 9 days, respectively. The worms were then collected and quickly frozen with liquid nitrogen.

Nile Red staining

Nile Red was dissolved with acetone at a final concentration of 0.5 mg/ml and then filtered with 0.22 μm filter. After washed for three times, J2 worms were added into 0.25× M9 buffer with 1% paraformaldehyde and rotated overnight. These fixed worms were washed with 0.25× M9 buffer three times and transferred to 1 ml 0.25× M9 buffer. Then, 6 μl of Nile Red solution was added into the buffer. After 12 h of incubation, worms were washed seven times with 0.25× M9 buffer. Determinations of Nile Red were made using a 460 nm, 35 nm bandpass excitation filter, and a 510 nm, 290 nm bandpass emission filter in a fluorescence microscope. At least, 15 nematodes were counted per assay, and all experiments were performed three times independently. Image-Pro Plus 6.0 software was used to quantify the fluorescence intensity of Nile Red.

Sudan Black B staining

Sudan Black B staining was carried out as described previously (41). Briefly, J2 worms were fixed with 2% paraformaldehyde in 0.25× M9 buffer for 1 h. These fixed worms then were washed three times with 0.25× M9 buffer to discard the residual of paraformaldehyde followed by three freeze/thaw cycles. Then, the worms were dehydrated using ethanol with concentrations of 25%, 50%, and 70%, respectively. These dehydrated worms were incubated in 70% ethanol containing Sudan Black B at 50% saturation overnight. At least, 15 nematodes were counted to quantify the intensity of Sudan Black B per assay, and all experiments were performed three times independently.

Oil Red O staining

Oil Red O staining was performed as described by O'Rourke with modification (42). Briefly, after washing three times with 0.25× PBS buffer, J2 worms were suspended in 400 μl 0.25× PBS. To fix the worms, 500 μl of 2× MRWB (1 mM spermidine-HCl, 0.4 mM spermine, 160 mM KCl, 40 mM NaCl, 14 mM Na_2EGTA, 0.2% β-mercaptoethanol, and 30 mM Na-Pipes at pH 7.4) and 100 μl of 20% paraformaldehyde were added into worms suspension. After 60 min of incubation, the worms were washed with 0.25× PBS five times and then dehydrated in 60% isopropanol for 10 min. Then, the worms were stained with filtered Oil Red O solution (60% Oil Red O isopropanol solution (5 mg/ml)/40% water) overnight. At least, 15 worms were randomly selected for photograph. Oil Red O intensities of individual worms were quantified with Image-Pro Plus 6.0 software. All experiments were performed three times independently.

Lysosome staining

After washing for three times, J2 worms were suspended in 0.25× M9 buffer. Then LysoTracker Red (DND-99) or Green (DND-26) dyes were added into worms suspension at a final concentration of 1 μM. The mixture was gently rotated at room temperature in the dark for 12 h. After washing with 0.25× M9 buffer five times, photographs of at least 15 worms were taken using fluorescence microscope. The fluorescence of LysoTracker Red was detected using a 530 nm, 20 nm bandpass excitation filter, and a 575 nm, 225 nm bandpass emission filter. Determinations of LysoTracker Green were made using

a 460 nm, 35 nm bandpass excitation filter, and a 510 nm, 290 nm bandpass emission filter. All experiments were performed three times independently.

Colocalization of lipid droplets and lysosome granules

To observe the colocalization of lipid droplets and lysosome granules, J2 worms were suspended in 0.25× M9 buffer with LysoTracker Green (DND-26) dyes at a final concentration of 1 μM for 12 h. After washing with 0.25× M9 buffer three times, the worms were fixed and stained by Nile Red dye as described above. Then, the worms were randomly selected for photographs fluorescence microscope using a 460 nm, 35 nm bandpass excitation filter, and a 510 nm, 290 nm bandpass emission filter.

Gene set enrichment analysis of differentially expressed genes

When living outside of hosts for 2 and 9 days (namely refer to early-, and middle-stage, respectively), J2 worms were collected and immediately frozen in liquid nitrogen, respectively. Quick-frozen early-, and middle-stage J2 worms were sent to Novogene Corporation for RNA-seq analysis to generate gene expression dataset. Gene Set Enrichment Analysis (4.1.0) software was downloaded from https://www.broadinstitute.org/gsea/. As described by Reimand *et al.* (43), KEGG pathway was performed with GSEA using gene expression dataset.

Electron microscopy

Electron microscopy of J2 worms was performed as described by Settembre *et al.* (29) and Zhang *et al.* (44). Briefly, after washing with 0.25× M9 buffer three times, the worms were fixed by 2.5% glutaraldehyde in PBS overnight at 4 °C. At the initiation of fixation, a surgical blade was used to cut worms into half under dissecting microscope. The worms were postfixed with 1% OsO_4 at 4 °C for 2 h and then dehydrated with serial ethanol to be embedded in Epon 812 resin. Sections at approximately 60 nm in thicknesses of worms embedded in Epon 812 resin were generated through a Leica EM UC7 ultramicrotome. The ultrathin sections were stained with 2% uranyl acetate and lead citrate and loaded onto Cu grids with 100 mesh. Electron micrographs of ultrathin sections were taken by a JEM 1400 plus transmission electron microscope at 120 KV.

Gas chromatography/mass spectrometry determination of fatty acid compositions

Fatty-acid composition in J2 worms was measured by producing fatty-acid methyl esters (FAMEs) as previously described (45). Briefly, worms were collected and washed with 0.25× M9 buffer for five times. One milliliter of 2.5% H_2SO_4 in methanol was added into worm pellet and then heated in water bath at 70 °C for 60 min to form FAMEs. Then, the tube was removed from water bath and kept at room temperature for 5 min. After addition of 0.2 ml hexane and 1.5 ml sterile water, FAMEs were extracted into the hexane layer by shaking vigorously and centrifuging the tubes at 3700 rmp. One hundred microliters of top hexane layer (this contains FAMEs) were carefully pipetted out and placed in a new tube for subsequent GC-MS analysis.

To determine fatty acid compositions, 2 μl of FAMEs in triplicate was injected into a Shimadzu GC/MS-QP2010 Ultra spectrometer (Shimadzu Scientific Instruments) equipped with a mass spectrometry with an electron impact ion source. Gas chromatography separation was performed by using an Agilent DB-WAX capillary GC column (30 m × 0.25 mm and 0.25 μm film thickness). The gas chromatography analysis was programmed for an initial temperature of 120 °C for 1 min followed by an increase of 10 °C/min to 190 °C. The column temperature was held for 8 min at 190 °C and then increased to 200 °C (2 °C/min) and kept for 2 min. The column was then increased to 220 °C (2 °C/min) and kept for 3 min. The mass spectrometry spectra were acquired with the electron impact voltage as tuning voltage. The mass range selected was 35 to 500 m/z. The relative amount of each FAME was calculated by comparing its peak area to the total areas. Fatty-acid abundance was expressed as the percentage of total fatty acids.

Construction of phylogenetic tree

Protein sequences of *C. elegans* homologs were downloaded from http://www.wormbase.org and protein sequences of *M. incognita* genes were downloaded from http://nematode.net. The remaining protein sequences were downloaded from http://www.ncbi.nlm.nih.gov. ClustalX was used to generate conserved domains of homologs in fasta and nexus formats (46). The aligned protein sequences were imported into ProtTest3.0 to generate parameters of best-fit models (47). The phylogenetic relationships among the analyzed genes and proteins were constructed based on the aligned sequences using MrBayes3.2 as described by Ronquist *et al.* (48). The statistical support for individual branches was determined using 10 million bootstrap runs.

Synthesis of dsRNA in vitro *and RNAi*

Total RNA was extracted using RNAprep Pure Micro Kit according to manufacturer's instructions (Tiangen Biotech). The first strand of cDNA was synthesized using PrimeScript 1st Strand cDNA Synthesis Kit (TaKaRa). Gene-specific primers containing couples of T7-labeled (Table S2) were carried out to generate templates for the synthesis of dsRNA. The corresponding dsRNA was synthesized using MEGAscript RNAi kit (Invitrogen, Thermo Fisher Scientific). An approximately 500 bp DNA fragment without sequence similarity with *M. incognita* genome was selected to generate negative control dsRNA.

Owing to the presence of stylet in plant parasitic nematodes, several neural stimulants are often added to stimulate the ingestion of dsRNA or siRNA. In this study, ingestion of dsRNA was performed according to the method as described by Huang *et al.* (49) and Adam *et al.* (50) with some modifications. Briefly, freshly hatched J2 of *M. incognita* were incubated with 0.25× M9 buffer that contained 0.05% gelatin, 0.5 mg/ml carbamoylcholine chloride, and 3 mM spermidine

for 8 h in the dark at room temperature on a rotary shaker. After gently washing three times with 0.25× M9 buffer without carbamoylcholine chloride, the worms were incubated in 0.25× M9 buffer containing 0.05% gelatin, 0.8 to 2 mg/ml dsRNA, 0.1 mg/ml FITC isomer I, and 3 mM spermidine for 24 h in the dark at room temperature on rotary shaker. The worms were gently washed with 0.25× M9 buffer three times for the following experiments.

Quantitative real-time PCR

Total RNAs were extracted from J2 worms with RNAprep Pure Micro Kit (Tiangen Biotech). Random-primed cDNA were generated by reverse transcription from total RNA with PrimeScript 1st Strand cDNA Synthesis Kit (TaKaRa). Quantitative real-time PCR was performed using LightCycler 480 SYBR Green I Master on a Roche LightCycler 480 System (Roche Applied Science). As described by Huang *et al.* (49), the actin gene (GenBank accession no. BE225475) was used as an internal control. The primers used for PCR were as follows: Minc16372 (*lipl-1*): 5′-TGG GAA ATG TTA GAG GCA ATC T-3′ (F) and 5′-TGC TGG CAA ATC TAT GGA GGA C-3′ (R), Minc06859 (*cpr-3*): 5′-ACT CAA AAG CGC CCA AAA CCC-3′ (F) and 5′-CAA CTG CCC AAC AAT CCC CAC-3′ (R), Minc05115 (*cpr-4*): 5′-TGG TCC TCT TCC TAC GCC TAA A-3′ (F) and 5′-CGC CTG GAA TAA CAC CTG TCG A-3′ (R), Minc05000 (*cpz-1*): 5′-GAC CGG AAC CAG CAT ATA CCT C-3′ (F) and 5′-CCA ACA TCT CCA CCT TCA CAG C-3′ (R), Minc00222 (*fat-6*): 5′-CGG CAG CAT TGT TTC GTT AT-3′ (F) and 5′-CAT GGA CTC GGT AGC TTT GAT-3′ (R), Minc00824 (*fat-3*): 5′-ATT TTT TGC TTT TTG GTT ACA ATA-3′ (F) and 5′-GAT TTT TGG TGG GTT GGT GAT-3′ (R), Minc10964 (*fat-4*): 5′-GCT GCT ACA AAT ATA GAC GGT AGA G-3′ (F) and 5′-TAA ATG TTG AAA AGG AAT TAA TCG A-3′ (R), Minc12955 (*elo-1*): 5′-TCT TCC TTC ATG CCT ATG TGT T-3′ (F) and 5′-TTT GAT TGT TCA TCC TTT TTT G-3′ (R), Minc08733b (*hlh-30b*): 5′-GGA GGT GGT GGT TTT GCT TTG T-3′ (F) and 5′-CCT TTT TCG ACT TTT CCG TTT T-3′ (R), and *actin*: 5′-GAT CCT CAC TGA ACG TGG TTA TTC T-3′ (F), and 5′-TCC TTG ATG TCA CGG ACA TCT C-3′ (R).

Lifespan analysis

After RNAi and NH_4Cl treatment as described above, J2 worms were equally divided into at least 25 aliquots. Each aliquot of about 200 of J2 worms were cultivated in sextuplicates to 35 mm Cell and Tissue Culture Dishes (Nest Biotechnology Co, Ltd) containing 3 ml 0.25× M9 buffer. Worms in 3 min unable to curve or bend when added with 300 μl of 1 M NaOH were judged as death (51). At every 24 h interval, the treated nematodes were counted under an Olympus SZ X16 microscope.

Assay of migration and body bending

For migration analysis, glass columns (5 mm internal diameter) sealed at one end with nylon net (300 mesh) and containing 50 mm moistened sand (grain diameter 0.25–1.0 mm) were placed vertically in a Costar 24 Well Cell Culture Cluster (Corning Incorporated) as described previously (52). One milliliter of 0.25× M9 buffer was added to the tube and sand column. Then, approximately, 120 of J2 worms were added into glass columns. After 24 h, these worms in individual well were counted. For body bending, approximately 20 of J2 worms were randomly selected and observed under microscope. An intact cycle of sinusoid or cosine was counted in 1 min for worms.

Infectivity assay

After soaked in water overnight at 28 °C, seeds of susceptible *Solanum lycopersicum* were transferred onto moist filter paper and then incubated at 28 °C for 3 days. When the roots of germinating seeds reached about 1 cm in length, young plants were transplanted into 23% pluronic gel in six Well Cell Culture Cluster at 16 °C. About 120 μl of packed J2 worms from individual experiments were pipetted onto a pluronic gel (about 300 of J2 worms per plant). Then, the six Well Cell Culture Cluster was put into an incubator at 28 °C for 36 h. To visualize and count J2 worms within roots, infected roots were stained with acid fuchsin as previously described (53, 54). The roots were viewed with microscope. All experiments were performed at least three times independently.

Statistics

These results presented in each figure are mean ± SD of three independent experiments performed at least in triplicate. Differences in gene expression, lipid content, median lifespan, migration rate, body bending, fluorescence intensity, and infectivity were analyzed by t tests or one-way ANOVA followed by Bonferroni correction post-tests. The data were analyzed using GraphPad Prism Version 8 package for Windows (GraphPad Software, Inc).

Data availability

All RNA-seq data are available in the GEO DataSets databases (https://www.ncbi.nlm.nih.gov/geo/query/acc.cgi?acc) under accession numbers GSE168150. All other relevant data are included in the article and its supporting information files.

Supporting information—This article contains supporting information.

Acknowledgments—We thank Dr Heng Jian (China Agricultural University) for *M. incognita* strain. We are grateful to Dr Jianping Xu (McMaster University, Canada) for his critical reading of this article and Dr Bin Liang (Yunnan University) for his technical assistance for GC-MS. This work was supported by a grant from the National Natural Science Foundation of China (U1802233), a Joint project from the Ministry of Education of PR China & Yunnan University (C176280101), and a grant from the Department of Science and Technology of Yunnan Province (202102AE090042-02-08).

Author contributions—C.-J. L., C.-G. Z., and K.-Q. Z. methodology; C.-J. L., C.-G. Z., and K.-Q. Z. formal analysis; C.-J. L., Y. M., Y.-L. W., T. Z., and G.-F. Y. investigation; C.-J. L., C.-G. Z., and K.-Q. Z.

data interpretation; M.-H. M. and K.-F. J. resources; L.-M. L. supervision; C.-J. L., C.-G. Z., and K.-Q. Z. writing–original draft.

Conflict of interest—The authors declare that they have no conflict of interest with the contents of this article.

Abbreviations—The abbreviations used are: AA, arachidonic acid; FAMEs, fatty-acid methyl esters; GSEA, gene set enrichment analysis; J2, second-stage juveniles; NHR, nuclear hormone receptor; PUFA, polyunsaturated fatty acid; qPCR, quantitative real-time PCR; RKNs, root-knot nematodes.

References

1. Chitwood, D. J. (2003) Research on plant-parasitic nematode biology conducted by the United States Department of Agriculture-Agricultural Research Service. *Pest Manag. Sci.* **59**, 748–753
2. Castagnone-Sereno, P., Danchin, E. G., Perfus-Barbeoch, L., and Abad, P. (2013) Diversity and evolution of root-knot nematodes, genus *Meloidogyne*: New insights from the genomic era. *Annu. Rev. Phytopathol.* **51**, 203–220
3. Ijani, A. S. M., Mabagala, R. B., and Nchimbi-Msolla, S. (2000) Efficacy of different control methods applied separately and in combination in managing root-knot nematodes (*Meloidogyne* spp.) in common beans. *Eur. J. Plant Pathol.* **106**, 1–10
4. Torto, B., Cortada, L., Murungi, L. K., Haukeland, S., and Coyne, D. L. (2018) Management of cyst and root knot nematodes: A chemical ecology perspective. *J. Agric. Food Chem.* **66**, 8672–8678
5. Abad, P., Gouzy, J., Aury, J. M., Castagnone-Sereno, P., Danchin, E. G., Deleury, E., Perfus-Barbeoch, L., Anthouard, V., Artiguenave, F., Blok, V. C., Caillaud, M. C., Coutinho, P. M., Dasilva, C., De Luca, F., Deau, F., *et al.* (2008) Genome sequence of the metazoan plant-parasitic nematode *Meloidogyne incognita*. *Nat. Biotechnol.* **26**, 909–915
6. Das, S., Wesemael, W. M. L., and Perry, R. N. (2011) Effect of temperature and time on the survival and energy reserves of juveniles of *Meloidogyne* spp. *Agric. Sci. Res. J.* **1**, 102–112
7. Barrett, J. (1968) Lipids of the infective and parasitic stages of some nematodes. *Nature* **218**, 1267–1268
8. Jo, H., Shim, J., Lee, J. H., Lee, J., and Kim, J. B. (2009) IRE-1 and HSP-4 contribute to energy homeostasis via fasting-induced lipases in *C. elegans*. *Cell Metab.* **9**, 440–448
9. O'Rourke, E. J., and Ruvkun, G. (2013) MXL-3 and HLH-30 transcriptionally link lipolysis and autophagy to nutrient availability. *Nat. Cell Biol.* **15**, 668–676
10. Tao, J., Ma, Y. C., Yang, Z. S., Zou, C. G., and Zhang, K. Q. (2016) Octopamine connects nutrient cues to lipid metabolism upon nutrient deprivation. *Sci. Adv.* **2**, e1501372
11. da Silva Rocha, F., Campos, V. P., Catão, H. C. R. M., Muniz, M. D. F. S., and Civil, N. (2015) Correlations among methods to estimate lipid reserves of second-stage juveniles and its relationships with infectivity and reproduction of *Meloidogyne incognita*. *Nematology* **17**, 345–352
12. Shivakumara, T. N., Dutta, T. K., Mandal, A., and Rao, U. (2019) Estimation of lipid reserves in different life stages of *Meloidogyne incognita* using image analysis of Nile Red-stained nematodes. *Nematology* **21**, 267–274
13. Goodell, P. B., and Ferris, H. (1989) Influence of environmental factors on the hatch and survival of *Meloidogyne incognita*. *J. Nematol.* **21**, 328–334
14. Storey, R. M. J. (1984) The relationship between neutral lipid reserves and infectivity for hatched and dormant juveniles of *Globodera* spp. *Ann. Appl. Biol.* **104**, 511–520
15. Patel, M., Stolinski, M., and Wright, D. (1997) Neutral lipids and the assessment of infectivity in entomopathogenic nematodes: Observations on four *Steinernema* species. *Parasitology* **114**, 489–496
16. da Silva Rocha, F., Campos, V. P., and De Souza, J. T. (2010) Variation in lipid reserves of second-stage juveniles of *Meloidogyne exigua* in a coffee field and its relationship with infectivity. *Nematology* **12**, 365–371
17. Ruaud, A. F., Nilsson, L., Richard, F., Larsen, M. K., and Tuck, S. (2010) The *C. elegans* P4-ATPase TAT-1 regulates lysosome biogenesis and endocytosis. *Traffic* **10**, 88–100
18. Jie, C., Ou, Y., Yi, L., Hu, S., Shao, L. W., and Liu, Y. (2017) Metformin extends *C. elegans* lifespan through lysosomal pathway. *Elife* **6**, e31268
19. Wang, Z., Zhao, H., Yuan, C., Zhao, D., and Zhang, H. (2019) The RBG-1/RBG-2 complex modulates autophagy activity by regulating lysosomal biogenesis and function. *J. Cell Sci.* **132**, jcs.234195
20. Settembre, C., Fraldi, A., Medina, D. L., and Ballabio, A. (2013) Signals from the lysosome: A control centre for cellular clearance and energy metabolism. *Nat. Rev. Mol. Cell Biol.* **14**, 283–296
21. Lapierre, L. R., De Magalhaes Filho, C. D., Mcquary, P. R., Chu, C. C., Visvikis, O., Chang, J. T., Gelino, S., Ong, B., Davis, A. E., and Irazoqui, J. E. (2013) The TFEB orthologue HLH-30 regulates autophagy and modulates longevity in *Caenorhabditis elegans*. *Nat. Commun.* **4**, 1–8
22. Settembre, C., Di Malta, C., Polito, V. A., Arencibia, M. G., Vetrini, F., Erdin, S., Erdin, S. U., Huynh, T., Medina, D., and Colella, P. (2011) TFEB links autophagy to lysosomal biogenesis. *Science* **332**, 1429–1433
23. Barker, K. R., Carter, C. C., and Sasser, J. N. (1989) An advance treatise on meloidogyne. In *Methodology* (Vol. 1,. North Carolina State University Graphics, Raleigh, NC: 47–78. Biology and Control
24. Schulze, R. J., Krueger, E. W., Weller, S. G., Johnson, K. M., Casey, C. A., Schott, M. B., and McNiven, M. A. (2020) Direct lysosome-based autophagy of lipid droplets in hepatocytes. *Proc. Natl. Acad. Sci. U. S. A.* **117**, 32443–32452
25. Grove, C. A., De Masi, F., Barrasa, M. I., Newburger, D. E., Alkema, M. J., Bulyk, M. L., and Walhout, A. J. (2009) A multiparameter network reveals extensive divergence between *C. elegans* bHLH transcription factors. *Cell* **138**, 314–327
26. Watts, J. L. (2002) Genetic dissection of polyunsaturated fatty acid synthesis in Caenorhabditis elegans. *Proc. Natl. Acad. Sci. U. S. A.* **99**, 5854–5859
27. Gundy, S. D. V., Bird, A. F., and Wallace, H. R. (1967) Aging and starvation in larvae of *Meloidogyne javanica* and *Tylenchulus semipenetrans*. *Phytopathology* **57**, 559–571
28. Christophers, A., Benson, J., Evans, A., Patel, M., Wright, D., and Saka, V. (1997) A rapid field-laboratory bioassay to assess the infectivity of *Meloidogyne* spp. second stage juveniles. *Nematologica* **43**, 117–120
29. Settembre, C., De Cegli, R., Mansueto, G., Saha, P. K., Vetrini, F., Visvikis, O., Huynh, T., Carissimo, A., Palmer, D., Klisch, T. J., Wollenberg, A. C., Di Bernardo, D., Chan, L., Irazoqui, J. E., and Ballabio, A. (2013) TFEB controls cellular lipid metabolism through a starvation-induced autoregulatory loop. *Nat. Cell Biol.* **15**, 647–658
30. Ghosh, A., Jana, M., Modi, K., Gonzalez, F. J., Sims, K. B., Berry-Kravis, E., and Pahan, K. (2015) Activation of peroxisome proliferator-activated receptor α induces lysosomal biogenesis in brain cells. *J. Biol. Chem.* **290**, 10309–10324
31. Folick, A., Oakley, H. D., Yu, Y., Armstrong, E. H., Kumari, M., Sanor, L., Moore, D. D., Ortlund, E. A., Zechner, R., and Wang, M. C. (2015) Aging. Lysosomal signaling molecules regulate longevity in *Caenorhabditis elegans*. *Science* **347**, 83–86
32. Robinson-Rechavi, M., Maina, C. V., Gissendanner, C. R., Laudet, V., and Sluder, A. (2005) Explosive lineage-specific expansion of the orphan nuclear receptor HNF4 in nematodes. *J. Mol. Evol.* **60**, 577–586
33. Pathare, P. P., Lin, A., Bornfeldt, K. E., Taubert, S., and Van Gilst, M. R. (2012) Coordinate regulation of lipid metabolism by novel nuclear receptor partnerships. *PLoS Genet.* **8**, e1002645
34. Ratnappan, R., Amrit, F. R., Chen, S.-W., Gill, H., Holden, K., Ward, J., Yamamoto, K. R., Olsen, C. P., and Ghazi, A. (2014) Germline signals deploy NHR-49 to modulate fatty-acid β-oxidation and desaturation in somatic tissues of *C. elegans*. *PLoS Genet.* **10**, e1004829
35. Dhe-Paganon, S., Duda, K., Iwamoto, M., Chi, Y.-I., and Shoelson, S. E. (2002) Crystal structure of the HNF4α ligand binding domain in complex with endogenous fatty acid ligand. *J. Biol. Chem.* **277**, 37973–37976
36. Wisely, G. B., Miller, A. B., Davis, R. G., Thornquest, A. D., Jr., Johnson, R., Spitzer, T., Sefler, A., Shearer, B., Moore, J. T., and Miller, A. B. (2002) Hepatocyte nuclear factor 4 is a transcription factor that constitutively binds fatty acids. *Structure* **10**, 1225–1234

37. Oka, Y., and Pivonia, S. (2002) Use of ammonia-releasing compounds for control of the root-knot nematode *Meloidogyne javanica*. *Nematology* **4**, 65–71
38. Su, L., Ruan, Y., Yang, X., Wang, K., Li, R., and Shen, Q. (2015) Suppression on plant-parasitic nematodes using a soil fumigation strategy based on ammonium bicarbonate and its effects on the nematode community. *Sci. Rep.* **5**, 1–13
39. Oteifa, B. A. (1955) Nitrogen source of the host nutrition in relation to infection by a root-knot nematode, *Meloidogyne incognita*. *Plant Dis.* **39**, 902–903
40. Perry, R. N., and Wharton, D. A. (2011) *Molecular and Physiological Basis of Nematode Survival*, CABI, Wallingford, UK
41. Narbonne, P., and Roy, R. (2009) *Caenorhabditis elegans* dauers need LKB1/AMPK to ration lipid reserves and ensure long-term survival. *Nature* **457**, 210–214
42. O'Rourke, E. J., Soukas, A. A., Carr, C. E., and Ruvkun, G. (2009) *C. elegans* major fats are stored in vesicles distinct from lysosome-related organelles. *Cell Metab.* **10**, 430–435
43. Reimand, J., Isserlin, R., Voisin, V., Kucera, M., Tannus-Lopes, C., Rostamianfar, A., Wadi, L., Meyer, M., Wong, J., Xu, C. J., Merico, D., and Bader, G. D. (2019) Pathway enrichment analysis and visualization of omics data using g:Profiler, GSEA, Cytoscape and EnrichmentMap. *Nat. Protoc.* **14**, 482–517
44. Zhang, S. O., Box, A. C., Xu, N., Le Men, J., Yu, J., Guo, F., Trimble, R., and Mak, H. Y. (2010) Genetic and dietary regulation of lipid droplet expansion in *Caenorhabditis elegans*. *Proc. Natl. Acad. Sci. U. S. A.* **107**, 4640–4645
45. Chen, Y. L., Tao, J., Zhao, P. J., Tang, W., Xu, J. P., Zhang, K. Q., and Zou, C. G. (2019) Adiponectin receptor PAQR-2 signaling senses low temperature to promote *C. elegans* longevity by regulating autophagy. *Nat. Commun.* **10**, 2602
46. Thompson, J. D., Higgins, D. G., and Gibson, T. J. (1994) CLUSTAL W: Improving the sensitivity of progressive multiple sequence alignment through sequence weighting, position-specific gap penalties and weight matrix choice. *Nucleic Acids Res.* **22**, 4673–4680
47. Abascal, F., Zardoya, R., and Posada, D. (2005) ProtTest: Selection of best-fit models of protein evolution. *Bioinformatics* **21**, 2104–2105
48. Ronquist, F., Teslenko, M., van der Mark, P., Ayres, D. L., Darling, A., Hohna, S., Larget, B., Liu, L., Suchard, M. A., and Huelsenbeck, J. P. (2012) MrBayes 3.2: Efficient Bayesian phylogenetic inference and model choice across a large model space. *Syst. Biol.* **61**, 539–542
49. Huang, G., Allen, R., Davis, E. L., Baum, T. J., and Hussey, R. S. (2006) Engineering broad root-knot resistance in transgenic plants by RNAi silencing of a conserved and essential root-knot nematode parasitism gene. *Proc. Natl. Acad. Sci. U. S. A.* **103**, 14302–14306
50. Adam, M. A., Phillips, M. S., Jones, J. T., and Blok, V. C. (2008) Characterisation of the cellulose-binding protein *Mj-cbp-1* of the root knot nematode, *Meloidogyne javanica*. *Physiol. Mol. Plant Pathol.* **72**, 21–28
51. Chen, S. Y., and Dickson, D. W. (2000) A technique for determining live second-stage juveniles of *Heterodera glycines*. *J. Nematol.* **32**, 117–121
52. Dalzell, J. J., McMaster, S., Fleming, C. C., and Maule, A. G. (2010) Short interfering RNA-mediated gene silencing in *Globodera pallida* and *Meloidogyne incognita* infective stage juveniles. *Int. J. Parasitol.* **40**, 91–100
53. Dutta, T. K., Powers, S. J., Kerry, B. R., Gaur, H. S., and Curtis, R. H. (2011) Comparison of host recognition, invasion, development and reproduction of *Meloidogyne graminicola* and *M. incognita* on rice and tomato. *Nematology* **13**, 509–520
54. Bakhetia, M., Charlton, W., Atkinson, H. J., and McPherson, M. J. (2005) RNA interference of dual oxidase in the plant nematode *Meloidogyne incognita*. *Mol. Plant Microbe* **18**, 1099–1106